Magnetization dynamics in interlayer exchange-coupled in-plane/out-of-plane anisotropy bilayers

N. Vukadinovic*
Dassault Aviation, 78 quai Marcel Dassault, 92552 St-Cloud, France

J. Ben Youssef and V. Castel
UBO/LMB/CNRS-FRE 3117, 29285 Brest, France

M. Labrune
LPMTM, CNRS-UPR 9001, Institut Galilée, Université Paris-13, 93430 Villetaneuse, France
(Received 27 January 2009; revised manuscript received 31 March 2009; published 5 May 2009)

The static and high-frequency properties of bilayer systems consisting in a single-crystal garnet film with a perpendicular anisotropy exchange coupled with a thin Permalloy film with a small in-plane anisotropy have been investigated both numerically and experimentally. The dynamic susceptibility spectra computed by means of two-dimensional micromagnetic simulations extended to stratified films reveal clearly the existence of multiple resonance lines resulting from the coupling between different magnetic area (domain walls, domains) inside the garnet film and the Permalloy film. In particular, exaltation of intensive domain wall resonances occurs within the frequency range including the uniform gyromagnetic mode of the Permalloy film. The effect of the garnet and Permalloy film thicknesses on the features of the dynamic susceptibility spectra is then studied. The experimental power absorption spectra recorded on a Permalloy/YIGBiLuAl-like bilayer exhibit well-defined resonance lines, most of them assigned to coupled modes of the bilayer nicely predicted by the micromagnetic simulations. The strong direct exchange coupling at the interface between the two layers appears as a predominant factor for this metal-oxide system.

DOI: 10.1103/PhysRevB.79.184405 PACS number(s): 75.40.Gb, 75.40.Mg, 75.75.+a

I. INTRODUCTION

Numerous emerging magnetic components for high-density recording media, spintronics, sensors, and microwave devices are based on artificially structured materials. A common architecture encountered in these systems corresponds to multilayered structures for which the proximity effect between the layers leads to magnetic properties unreachable to standard single-layer systems.[1] In this context, a deep understanding of the magnetic coupling between the constitutive layers and of the consequences on the static and dynamic properties become of crucial interest.

Among the multitude of the investigated magnetic stacks, a rich system corresponds to all-ferromagnetic multilayers including films with a perpendicular anisotropy. In the simplest case, the magnetic properties of the multilayer are controlled by the competition between the long-range dipolar interaction, the short-range direct exchange coupling at each interface and, the local anisotropy interaction. The associated magnetic ground state can develop a nonuniform micromagnetic structure depending on the individual layer thicknesses and the amplitude of the perpendicular anisotropy fields. The periodic stripe domain structure represents an example of a nonuniform magnetization distribution appearing in such multilayers. Stripe domains were observed by magnetic force microscopy (MFM) in various ferromagnetic Co/Fe,[2] $Fe_{81}Ni_{19}$/Co,[3] and FePd (Ref. 4) multilayers and, in ferrimagnetic/ferromagnetic bilayers.[5] Furthermore, detailed analyses of the stripe domain structure within such multilayer films were performed by means of numerical simulations based on a two-dimensional (2D) static micromagnetic model. Nice agreement was found between theory and experiments in terms of stripe periodicity, remanent magnetization and saturation field for Co/Fe[6] and FePd.[4]

Bollero *et al.*[7] have studied the static magnetic properties of NiFe films (in-plane anisotropy) coupled to [Pt/Co] multilayers (out-of-plane anisotropy) using MFM imaging, extraordinary Hall effect (hysteresis loops), and micromagnetic simulations. It was emphasized that the presence of unequal closure domains at the interface between the [Pt/Co] multilayer and the NiFe film, created after in-plane saturation, is responsible for the shift in the in-plane hysteresis loop experimentally evidenced. In addition, the amplitude of this exchange biaslike effect (EB-like effect) can be controlled through the number of Pt/Co repetitions in the multilayer and the NiFe film thickness which affect the structure of the closure domains. On the other hand, the static and dynamic properties of Co/Fe multilayers were also recently studied.[8] A stripe domain pattern can develop in such multilayers, the features of which depend on the respective thicknesses of the layer, the number of replications of the Co/Fe bilayer, and the amplitude of the respective anisotropy fields. From the dynamic point of view, the anisotropy contrast between the layers leads to a localization of magnetic modes within the soft layers (Fe films).

The metal-oxide multilayers represent another class of systems of interest. The open question is to identify the nature of the interlayer magnetic coupling between the metallic and the oxide layers. The type of coupling depends on the nature of the magnetic materials and on the growth techniques. Recent works were reported on bilayers consisting of Fe films ion beam sputtered on yttrium iron garnet (YIG)-like underlayers having a perpendicular anisotropy.[5] The static magnetic properties of the bilayers were investigated by means of MFM, magneto-optic Kerr effect (hysteresis loops), and micromagnetic simulations. As a result, it was

demonstrated that the Fe film exhibits a perpendicular anisotropy for a Fe film thickness lower than 20 nm. Within this thickness range, the stripe domain structure of the YIG-like film is replicated in the Fe film due to the presence of a strong interlayer exchange coupling.

The purpose of the present paper is to investigate the interlayer exchange coupling between a single-crystal garnet film with a perpendicular anisotropy and a $Ni_{80}Fe_{20}$ (Permalloy noted hereafter Py) overcoat with a small in-plane anisotropy through the magnetization dynamics of the bilayer. The paper is organized as follows: Sec. II presents a numerical analysis of the static and dynamic properties of the bilayer carried out by means of 2D micromagnetic simulations. The assumption of a strong direct exchange coupling at the interface between the two layers results in an in-plane dynamic susceptibility spectrum transverse to the stripe direction with multiple resonance lines originating from coupled modes between the Py film and the domain wall (DW) inside the garnet film. The effects of the respective film thicknesses on the features of the dynamic susceptibility spectrum are reported. Section III is devoted to the experimental data obtained from wide band microwave measurements and the comparisons with the theoretical predictions. Lastly, some outlooks are drawn from the obtained results.

II. MICROMAGNETIC SIMULATIONS

A. Model

The frequency dependence of the full dynamic susceptibility tensor $\bar{\bar{\chi}}$ is computed by using a two-dimensional micromagnetic model. This one, described elsewhere,[9] is based on the solution in the frequency domain of the Landau-Lifshitz-Gilbert equation for magnetization motion linearized around the equilibrium configuration. The effective field $\mathbf{H}_{\text{eff}}$ incorporates the contributions from the exchange, anisotropy, demagnetizing, and dc applied magnetic fields. The magnetic systems are assumed invariant along one direction (z axis), periodic along the second direction (x axis) and of finite thickness along the third direction (y axis). This model is well adapted for probing the dynamic response of nonuniform and periodic equilibrium magnetization configurations as those encountered in single-layer films with stripe domains (the z axis coincides with the stripe direction).

In order to treat the case of multilayer films with nonuniform magnetization distributions, this model has been extended. Each magnetic layer i is described by its thickness t_i and the following magnetic parameters: the exchange constant A_i, the saturation magnetization $M_{S,i}$, one or several volume anisotropy constants $K_{\beta,i}(\beta=,1,2,\ldots)$ according to the crystal symmetry, the gyromagnetic ratio γ_i and the Gilbert damping parameter α_i.

In the general case, the Hoffmann boundary conditions[10,11] have to be fulfilled along the interface between the two magnetic layers, denoted i and j. These conditions read

$$\mathbf{m}_i \times \left[2A_i \frac{\partial \mathbf{m}_i}{\partial \mathbf{n}_i} + \nabla_{mi} E_{\text{int},i} - J\mathbf{m}_j\right] = \mathbf{0}$$

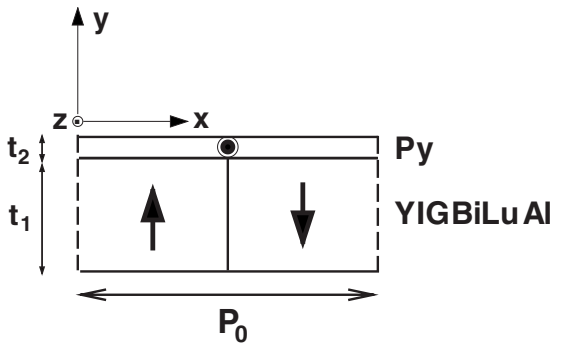

FIG. 1. Schematic representation of the Py/YIGBiLuAl bilayer over one period P_0 of the stripe pattern and coordinate system. A single-crystal YIGBiLuAl film of thickness t_1 with a perpendicular anisotropy is covered by a Py overlayer of thickness t_2 ($t_2 \ll t_1$) with an in-plane anisotropy.

$$\mathbf{m}_j \times \left[2A_j \frac{\partial \mathbf{m}_j}{\partial \mathbf{n}_j} + \nabla_{mj} E_{\text{int},j} - J\mathbf{m}_i\right] = \mathbf{0}, \tag{1}$$

where $\mathbf{m}_k = \mathbf{M}_k / M_{S,k}$, $k=i,j$, $\mathbf{n}_k$, $k=i,j$, is the outward normal of the kth layer, $E_{\text{int},k}$, $k=i,j$ is the interface anisotropy energy density and J is the interlayer exchange coupling for an interfacial exchange energy density of the bilinear form $E_{\text{ex,int}} = -J\mathbf{m}_i \cdot \mathbf{m}_j$.

For $J=0$, Eq. (1) transforms into the Rado-Weertmann[12] boundary condition. If the interface anisotropy energy is also zero, Eq. (1) yields the free boundary condition $\partial \mathbf{m} / \partial \mathbf{n} = \mathbf{0}$ where $\mathbf{n}_i = -\mathbf{n}_j = \mathbf{n}$. This condition will be used for the two external surfaces.

For layers in direct contact, a strong interlayer exchange coupling is expected.[5,13] Our model accounts for this point and it is based on the following conditions:

(i) In the limit of a strong exchange coupling[14] (large values of J), the magnetization of the two layers at the interface are locked together. This leads to the continuity of the reduced magnetization, namely,

$$\mathbf{m}_i = \mathbf{m}_j, \tag{2}$$

(ii) The interface anisotropy energy is neglected. Its contribution is thought to be weak with respect to the one of interlayer exchange energy.

Under these assumptions, the general solution of Eq. (1) writes

$$A_i \frac{\partial \mathbf{m}_i}{\partial \mathbf{n}} = A_j \frac{\partial \mathbf{m}_j}{\partial \mathbf{n}}. \tag{3}$$

It should be remarked that the interlayer exchange constant J disappears in this expression and only the bulk exchange constant of each layer subsists. A rough estimate of the value J_l corresponding to the limit of a strong exchange coupling can be obtained using Eq. (27) in Ref. 14. For the bilayers considered hereafter, J_l is around 10 erg/cm^2.

The bilayer films under consideration consist in a single-crystal garnet film (YIGBiLuAl-like) of thickness t_1 with a perpendicular uniaxial anisotropy (constant K_u) overcoated by a Py film of thickness t_2 with an in-plane uniaxial anisotropy (constant K_p) as displayed in Fig. 1 for one period P_0

TABLE I. Set of magnetic parameters for the Py/YIGBiLuAl bilayers used for the micromagnetic simulations.

	A (emu/cm)	M_s (emu/cm^3)	K_u (erg/cm^3)	K_p (erg/cm^3)	γ (s^{-1} Oe^{-1})	α
YIGBiLuAl	2×10^{-7}	39.8	1.4×10^4	0	1.8×10^7	0.02
Py	10^{-6}	826.3	0	2×10^3	1.8×10^7	0.02

of the stripe pattern. It is noteworthy that this kind of Py/garnet composite structure was investigated during the period of extensive works on magnetic bubble films. Use of a Py overcoat was identified as a solution for suppressing the vertical Bloch lines within the bubbles.[15] This effect was ascribed to the strong exchange coupling across the Py/garnet interface.[16]

The magnetic parameters used for the micromagnetic simulations are gathered in Table I. It should be remarked that the cubic magnetocrystalline anisotropy of the YIGBiLuAl film has been neglected. Its magnitude (absolute value) is typically 1 order of magnitude lower than the one of the perpendicular uniaxial anisotropy.

The static and dynamic micromagnetic simulations were performed using mesh sizes satisfying the spatial discretization rules in the YIGBiLuAl film, namely, $\Delta_x \leq \Delta_0/3$, $\Delta_y \simeq 2\Delta_0/5$, $\Delta_0=(A/K_u)^{1/2}$ being the Bloch domain wall width parameter which is lower than the exchange length $[\Lambda=(A/2\pi M_S^2)^{1/2}]$ for materials with a quality factor $Q>1$, the quality factor being defined as $Q=K_u/2\pi M_S^2$. This criterium allows an accurate description of the static and dynamic behaviors of the thin domain walls in the garnet films. The constraint of using a uniform mesh leads to relax the discretization rules in the Py film. However, it was verified that this mesh size ensures the convergence of the static and dynamic micromagnetic simulations for thin films with a low-quality factor for which no rapid spatial variations in the micromagnetic structure are expected. The dynamic susceptibility spectra displayed thereafter correspond to the diagonal elements of the dynamic susceptibility tensor (imaginary part) averaged over the periodic cell and computed within the frequency range 0.02–3 GHz.

B. Results

In a first step, the static magnetic properties both for a YIGBiLuAl monolayer and for a Py/YIGBiLuAl bilayer are investigated using 2D static micromagnetic simulations.[17] The cross-sectional equilibrium magnetization configuration over one period of the stripe pattern for a 1-μm-thick YIGBiLuAl monolayer is displayed in Fig. 2(a) as a reference case. The color code images the m_x and the m_z components of the magnetization in the left and right columns, respectively. The arrows represent the component of **m** in the plane (Ox,Oy) perpendicular to the stripe direction $(Oz$ axis). The micromagnetic state consists in an open flux pattern with up and down domains magnetized along the $+y$ axis and the $-y$ axis, respectively. These domains are separated by a twisted DW with a Bloch character at the film center (see m_z component) and a Néel character at the film surfaces (see m_x component). The zero-field period of the stripe pattern is equal to $P_0=2$ μm corresponding to twice the film thickness. Adding a 30-nm-thick Py overcoat onto the YIGBiLuAl film results in deep changes in the static magnetization configuration as shown in Fig. 2(b). These modifications can be summarized as follows: (i) a noticeable asymmetry appears between the top and the bottom Néel caps (see left column). The top Néel cap is elongated along the x axis and contracted along the y axis with respect to the bottom Néel cap. (ii) The location of the Bloch DW core $(m_x=0)$ initially at the film center for the YIGBiLuAl monolayer is shifted toward the interface of the bilayer (see right column). (iii) The Py film allows to close the magnetic flux. The static magnetization within the Py film is indeed mainly oriented along the z axis

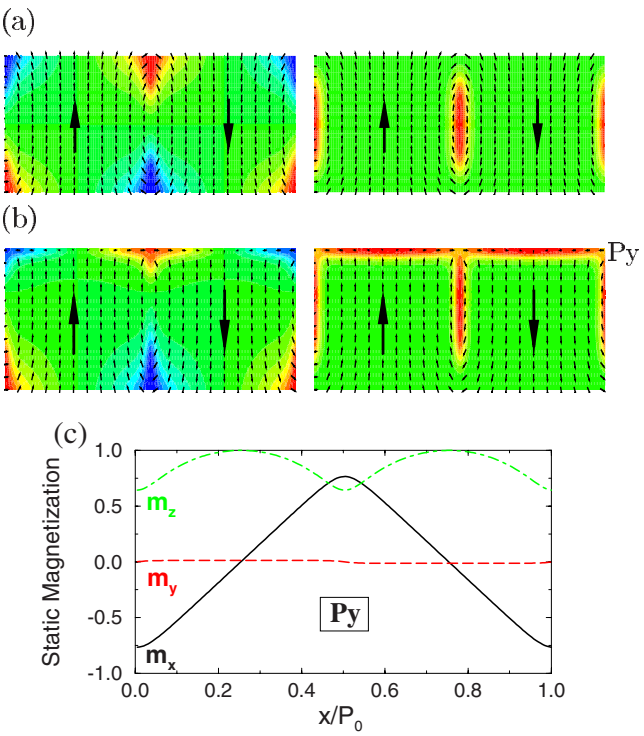

FIG. 2. (Color online) Equilibrium magnetization distributions computed by 2D static micromagnetic simulations. Cross-sectional views within one period of the domain pattern: (a) YIGBiLuAl monolayer, $t_1=1$ μm, and (b) Py/YIGBiLuAl bilayer, $t_1=1$ μm and $t_2=30$ nm. The arrows represent the component of the reduced magnetization **m** in the plane of the figure. A color code is adopted for imaging the magnetization component m_x (left column) and m_z (right column). The negative values appear in blue and the positive ones in red. (c) Static magnetization profile $m_i(x/P_0)$, $i=x,y,z$ inside the Py layer at the position $y=t_1+t_2-\Delta y/2$, Δy being the mesh size along the y axis.

at the upper surfaces of domains as reported in Fig. 2(c). As a consequence, the closure of the magnetic flux between the domains is essentially in the (Oy,Oz) plane for the upper surface whereas it is confined in the (Ox,Oy) plane for the lower surface. (iv) The zero-field stripe period is increased and is equal to $P_0=2.65$ μm. At this point, it seems interesting to discuss our results with respect to those reported in Ref. 7 for a NiFe film coupled to a [Co/Pt] multilayer. In this last case, the Py film thickness is lower than the exchange length and the saturation magnetization of the [Co/Pt] multilayer exceeds the one of the Py overlayer. The static domain structure corresponds to up and down segmented domains characterized by the equilibrium period P_0 far greater than the total thickness. The static micromagnetic simulations of this system in the remanent state after in-plane saturation indicated that the main role of the Py film assumed isotropic is to induce an enlargement of the top Néel cap in the [Co/Pt] multilayer. In addition, the micromagnetic structure of the Py film tends to reproduce the one of the [Co/Pt] multilayer (replication effect). For this system, the flux closure between the domains remains essentially in the (Ox,Oy) plane for both surfaces. In our case, the situation is quite different. The Py film thickness is greater than the exchange length and the saturation magnetization of the Py overlayer dominates largely the one of the YIGBiLuAl film. As a result, there is no replication of the YIGBiLuAl magnetic structure within the Py film. Due to the magnetostatic interaction, an in-plane orientation of the magnetization is imposed at the upper surface of the Py film. This constraint modifies the flux closure pattern at the upper surface of domains with a large m_z component leading to an asymmetry between the upper and lower flux closure planes and to the upward shift of the Bloch DW core as aforementioned.

The dynamic behavior of these mono- and bilayer systems is now explored. Figure 3 displays the dynamic susceptibility spectra (imaginary part of the diagonal element of the susceptibility tensor) within the frequency range 0.02–3 GHz for the YIGBiLuAl monolayer. This case is shown for comparison purposes. These spectra exhibit several well-separated resonance lines resulting from DW and domains excitations. The highest response is obtained for the χ''_{yy} spectrum. The spatial distribution of the dynamic susceptibility (modulus $|\chi_{\alpha\alpha}(x,y,z)|$, $\alpha=x,y,z$) within the periodic cell at each resonance frequency is displayed in the maps. These images reveal that the line (1) (resonance frequency $f_r=0.2$ GHz) arises from spins localized within the DW (mainly within the Bloch part of the DW for the χ''_{yy} spectrum, pumping field along the multilayer normal) whereas the line (6) ($f_r=0.24$ GHz) is associated with the Néel-like DW part (χ''_{zz} spectrum, pumping field along the stripe direction). Additional small-amplitude DW resonances at higher frequencies (lines 2, 3, and 7) related to flexural DW modes along the film thickness are also observed at higher frequencies. A detailed investigation of the DW excitations was previously reported[18] for single-crystal garnet films with $Q=1.5$. Domain resonance modes are observed within the frequency range 1.5–3 GHz. For each in-plane pumping field configuration, the low-frequency lying resonance lines (lines 4 and 8 at $f_r=1.47$ GHz and $f_r=1.62$ GHz, respectively) correspond to surface domain modes. At higher frequencies,

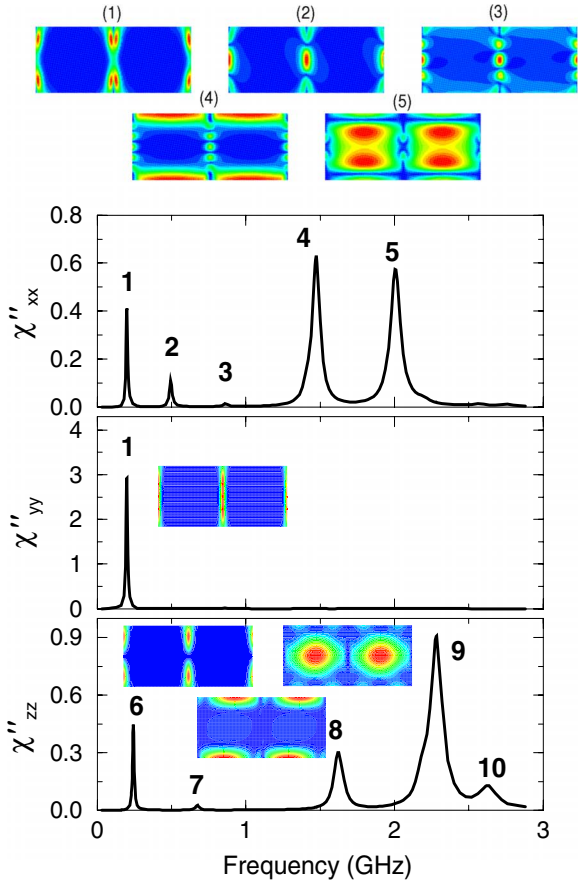

FIG. 3. (Color online) Dynamic susceptibility spectra (imaginary parts of the diagonal elements of the susceptibility tensor) for the YIGBiLuAl monolayer ($t_1=1$ μm) computed by 2D dynamic micromagnetic simulations. The color maps represent the spatial distribution of the modulus of the dynamic magnetization at each resonance frequency (high levels in red and low levels in blue).

volume domain mode resonances are observed (lines 5 and 9 at $f_r=2$ GHz and $f_r=2.28$ GHz, respectively). The resonance line 10($f_r=2.63$ GHz) is associated with a higher-order volume domain mode with periodic spatial variations along the domain width.

The dynamic susceptibility spectra for the Py/YIGBiLuAl bilayer ($t_1=1$ μm, $t_2=30$ nm) are reported in Fig. 4. One of the most striking features is the appearance of multiple resonant oscillations in the χ''_{xx} spectrum within the frequency range 0.2–2 GHz. The highest susceptibility levels are obtained for this pumping configuration. The analysis of the spatial distribution of the dynamic susceptibility at each resonance frequency allows to identify these different resonance lines (see the maps). The lines numbered from 1 to 8 are associated with coupled modes involving spin area localized within the DW of the YIGBiLuAl film and within the Py layer. The contribution of the Py layer grows with increasing the line index, passes through a maximum for the line 3 whose resonance frequency approaches the one of the uniform gyromagnetic mode for the Py film alone (see the χ''_{xx} spectrum for the Py film in the inset of the Fig. 4), and then decreases for the resonance lines at higher frequencies. The DW excitations within the garnet part of the bilayer corre-

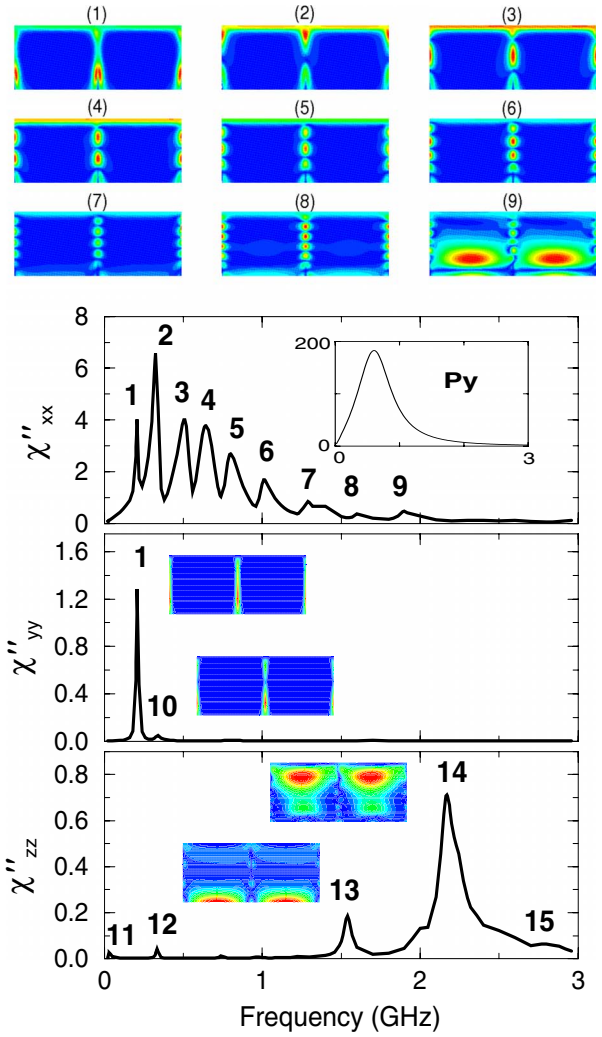

FIG. 4. (Color online) Dynamic susceptibility spectra for the Py/YIGBiLuAl bilayer (t_1=1 μm, t_2=30 nm) and spatial distribution of the dynamic magnetization at each resonance frequency computed by 2D dynamic micromagnetic simulations. The rule for imaging the resonance modes is the same as in Fig. 3. The standard response of a 30-nm-thick Py film with an in-plane magnetization along the z axis is recalled in the inset.

spond to flexion modes along the y axis. With respect to the YIGBiLuAl monolayer, new flexural modes (resonance lines 2 and 4) and higher-order flexural modes (resonance lines 6, 7, and 8) are detected. The resonance lines 1, 3, and 5 correspond to mode profiles that resemble those observed for the YIGBiLuAl single layer (resonance lines 1, 2, and 3 in Fig. 3), the presence of the Py overcoat inducing a symmetry breaking with respect to the midplane of the bilayer. The resonance frequencies of the lines 1, 3, and 5 are slightly modified (shifts lower than 10%) by the Py film with respect to corresponding modes in the YIGBiLuAl single layer. The resonance line 9 is assigned to the fundamental volume domain mode with also a strong asymmetry with respect to the midplane of the bilayer. Its resonance frequency is weakly lowered with respect to the case of the single layer. For the χ''_{yy} spectrum, the presence of the Py overcoat leads to the splitting of the fundamental Bloch-type DW resonance in two DW resonances with different mode profiles along the y axis. The low-frequency part of the χ''_{zz} spectrum is also affected by the existence of the Py film with the detection of two small-amplitude DW resonance lines (lines 11 and 12) instead of the main Néel-type DW resonance observed in the case of the YIGBiLuAl single layer. Domain resonances (lines 13, 14, and 15) still exist but their mode structure possesses a strong asymmetry with respect to the midplane of the bilayer. In short, adding a thin Py overcoat results in a strong exaltation of the DW resonances in the garnet film. It should be kept in mind that the previous dynamic behavior is based on the assumption of a strong direct exchange coupling between the two layers. Additional simulations (not presented here) performed by neglecting this interlayer exchange coupling show an increase in the zero-field stripe period and the disappearance of the multiple DW oscillations for the χ''_{xx} spectrum.

The effect of the YIGBiLuAl film thickness on the static and dynamic magnetic properties has been investigated. Figure 5(a) shows the zero-field stripe period evolution as a function of t_1 for both the single layer and the bilayer. In this last case, the Py film thickness is fixed at t_2=30 nm. For the single layer, P_0 increases with t_1. This evolution has been compared with the one deduced from the analytical model of Kooy and Enz[19] including the μ effect for taking into account the finite value of the Q factor. An increasing discrepancy appears for decreasing film thickness which probably reflects a static configuration far beyond the ideal situation of the Kooy and Enz model. For the bilayer system, P_0 increases more rapidly with t_1. For the thinnest garnet film, the stripe period is very weakly affected by the Py overcoat. Such a result is consistent with the one reported in Ref. 5 for the Fe/YIG system where the YIG film thickness is about 100 nm. Evolution of the χ''_{xx} spectrum for different YIGBiLuAl film thicknesses is reported in Figs. 5(b)–5(d). As a result, the number of absorption lines diminishes as t_1 decreases. The maps of the spatial distribution of the dynamic magnetization associated with each resonance line indicate that the observed modes for t_1=0.5 μm and t_1=0.25 μm resemble the first modes represented in Fig. 4 for the case t_1=1 μm. However, reducing t_1 induces a transformation of mode structures toward uncoupled modes. For example, the second mode for t_1=0.25 μm corresponds to the excitation of the Py film only whereas the third mode is assigned to a pure DW flexural mode similar to the one shown in Fig. 4 for the resonance line 3. As expected, the level of dynamic susceptibility is enhanced for increasing ratio t_2/t_1.

The effect of the Py film thickness on the static and dynamic magnetic properties of the bilayer is reported in Fig. 6. The evolution of the static magnetic profile $m_x(y/t)$ at the middle of the DW for different Py film thicknesses is drawn in Fig. 6(a). Starting from antisymmetric profile with respect to the midplane in the absence of the Py film, increasing t_2 yields the progressive reduction in the m_x component and hence of the upper Néel cap in the YIGBiLuAl film. In the Py film, the m_x component is approximately constant. As the Py film thickness increases, the m_z component increases. The magnetization inside the Py film is oriented along the Oz easy axis for the thickest Py film. It should be noticed that the zero-field stripe period is nearly constant as a function of

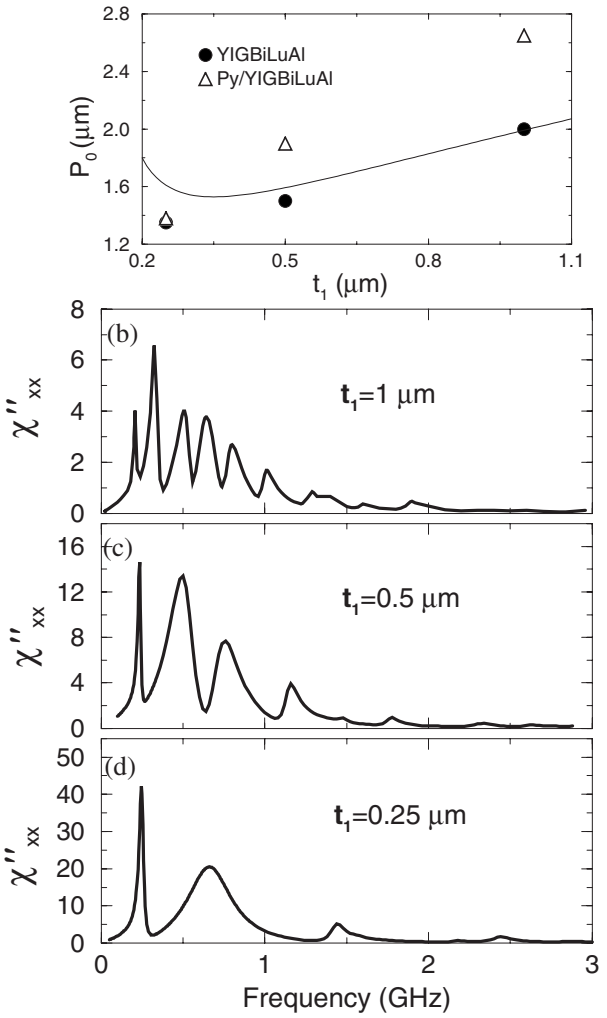

FIG. 5. Effect of the YIGBiLuAl film thickness on the static and dynamic behaviors of the Py/YIGBiLuAl bilayers computed by 2D micromagnetic simulations. (a) Zero-field stripe domain period P_0 as a function of the YIGBiLuAl film thickness without (filled circles) and with (open up triangles) an Py overlayer (t_2=30 nm). The solid line represents the evolution computed from the analytical Kooy and Enz model (Ref. 19) for a YIGBiLuAl monolayer. χ''_{xx} spectra: (b) t_1=1 μm, (c) t_1=0.5 μm, (d) t_1=0.25 μm. The thickness of the Py layer is fixed at t_2=30 nm.

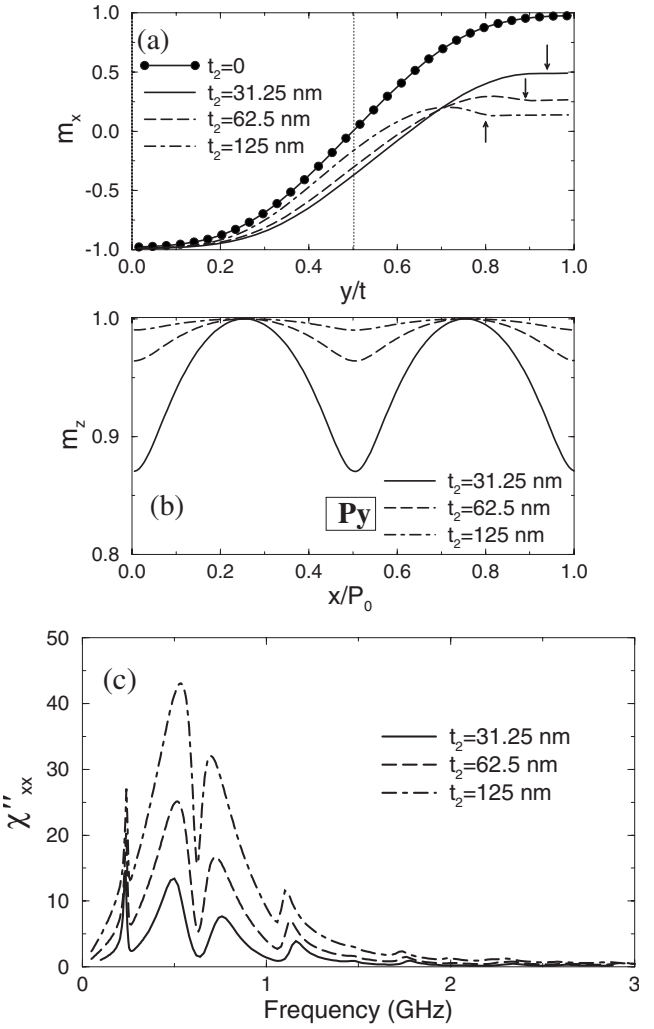

FIG. 6. Effect of the Py film thickness on the static and dynamic behaviors of the Py/YIGBiLuAl bilayers computed by 2D micromagnetic simulations: (a) static magnetization profiles $m_x(y/t)$ at the position $x=P_0/2$ (middle of the domain wall). The arrows delimit the boundary between the YIGBiGa (left side) and the Py (right side) layers. (b) Static magnetization profiles $m_z(x/P_0)$ inside the Py layer at the position $y=t_1+t_2-\Delta y/2$. (c) χ''_{xx} spectra. The thickness of the YIGBiGa film is fixed at t_1=0.5 μm.

t_2. The consequences on the χ''_{xx} spectrum are displayed in the Fig. 6(c). The number of resonant lines is kept constant whatever the Py film thickness. The main effect is the increase in the susceptibility level when the Py film thickness enhances. In addition, the gaps between the resonance lines diminish for increasing t_2. This spectrum tends toward the one of the Py film for a large Py thickness.

III. EXPERIMENTAL RESULTS

A. Materials

1. Sample preparation

Two types of sample were elaborated: a 0.5-μm-thick monolayer garnet film and a bilayer structure including a 0.5-μm-thick garnet film overcoated with a 30 nm thick Permalloy film. The single-crystal garnet films of nominal composition $(YBiLu)_3(FeAl)_5O_{12}$ were grown by liquid phase epitaxy (LPE) from a $PbO/Bi_2O_3/B_2O_3$ flux on (111)-oriented gadolinium gallium garnet (GGG) substrates. In order to achieve a large quality factor ($Q>1$), two strategies were employed. The Bi and Lu ions were selected for obtaining a large growth-induced uniaxial anisotropy characterized by the anisotropy constant $K_{u,g}$ which is the predominant contribution to the total uniaxial perpendicular anisotropy ($K_{u,g} \simeq K_u$).[20] In addition, the Al ions were substituted in Fe sites in order to reduce the saturation magnetization. The garnet films were obtained using the horizontal mode of dipping with an axial rotation at 60 rpm. The growth temperature was 830 °C. The growth rate was fixed at 0.3 μm/min in order to well control the film thickness and to optimize the magnetic parameters (saturation magnetization, uniaxial perpen-

TABLE II. Set of experimental magnetic parameters for the YIGBiLuAl and the Permalloy monolayers.

	M_s (emu/cm^3)	K_u (erg/cm^3)	K_p (erg/cm^3)	γ (s^{-1} Oe^{-1})	α
YIGBiLuAl	43.8	1.84×10^4	0	1.78×10^7	0.002
Py	826.3	0	1.78×10^3	1.85×10^7	0.008

dicular anisotropy). Due to the LPE growth process, two garnet films are simultaneously elaborated (one on each side of the GGG substrate), one of them being then removed.

For the bilayer system, a Permalloy thin film was deposited on the top of the garnet layer. This film was then covered by a 5-nm-thick Al_2O_3 layer in order to prevent the ferromagnetic film from oxydation. These two materials were grown by radio-frequency (RF) diode sputtering under the following conditions: a deposition pressure of 10^{-2} mbar and a RF power density of 4 W/cm^2. In addition, a dc magnetic field of 300 Oe was applied along the in-plane direction of the stripe domain in the garnet film ($[1,1,\bar{2}]$ axis) during deposition. This field plays a double role. First, it allows to induce a well-defined in-plane uniaxial anisotropy in the Permalloy film. Second, it imposes the collinearity between the easy axis of magnetization in the Permalloy film and the in-plane direction of the stripe domains in the garnet film.

2. Magnetic characterization

The magnetic parameters were determined from two reference samples: a 0.5-μm-thick $(YBiLu)_3(FeAl)_5O_{12}$ monolayer and a 30-nm-thick Permalloy monolayer. The saturation induction $4\pi M_S$ of samples was measured using a vibrating sample magnetometer (VSM). The in-plane uniaxial anisotropy constant K_p of the Permalloy film was extracted from the spectral position of the in-plane uniform gyromagnetic mode observed in the zero-field permeability spectrum recorded along the in-plane hard axis by means of a single coil permeameter.[21,22] Ferromagnetic resonance (FMR) measurements were also performed using a nonresonant wide band microstrip line over the frequency range 2–30 GHz. The uniaxial perpendicular anisotropy constant K_u and the gyromagnetic ratio γ were deduced from the linear frequency dependence of the resonance field for the uniform FMR mode in the perpendicular configuration (polarizing magnetic field applied along the film normal). The weak contribution of the cubic magnetocrystalline anisotropy will be neglected hereafter. The damping parameters α were deduced from the slope of the linear frequency dependence of the resonance linewidth associated with the uniform FMR mode in the perpendicular configuration. The identified magnetic parameters for the two samples are gathered in the Table II. The theoretical values of the exchange constant A were adopted namely, $A=2.10^{-7}$ erg/cm for the garnet film and $A=10^{-6}$ erg/cm for the Permalloy film.

The zero-field magnetic domain structures at the surface of the YIGBiLuAl monolayer and the Py/YIGBiLuAl bilayer were imaged by magnetic force microscopy (Fig. 7). For the YIGBiLuAl monolayer [Fig. 7(a)], the domain pattern consists in parallel stripe domains with the experimental zero-field period $P_{0,\mathrm{exp}}=1.49$ μm. This value is in agreement with the one deduced from the static micromagnetic simulation, $P_{0,\mathrm{ms}}=1.47$ μm. For the Py/YIGBiLuAl bilayer, the MFM image exhibits stripe domains with a weaker contrast [Fig. 7(b)]. With respect to the YIGBiLuAl monolayer, the stripe domains appear less regular and with an increased zero-field stripe period $P_{0,\mathrm{exp}}=1.9$ μm. The static micromagnetic simulation provides a quite similar result, $P_{0,\mathrm{ms}}=1.84$ μm. It should be remarked that the Py overcoat is in-plane magnetized as displayed in Fig. 2 and screens partly the stray field emerging from the garnet film which explains the relatively weak contrast of the MFM image. This situation differs from the one described in Ref. 5 regarding the Fe/YIG-like bilayer system. In this last case, the domain pattern observed by MFM results from the replication of the domain structure of the garnet film in the thinnest Fe overlayers (perpendicular magnetization inside the Fe films).

B. Power absorption spectra

Figure 8 displays the experimental and computed derivative rf power absorption dP_a/df versus frequency within the frequency range [0.1–3 GHz] for the YIGBiLuAl monolayer. The theoretical spectra were computed using a Gilbert damping parameter value $\alpha=0.008$ for the garnet film greater than the one deduced from FMR measurements in the saturated regime, $\alpha=0.002$ in order to have resonance linewidths near the experimental ones. Two orientations of the stripe domains with respect to the microstrip line are considered: stripe domains parallel (denoted parallel configuration)[Fig. 8(a)] or perpendicular (denoted perpendicular configuration) [Fig. 8(b)] to it. Due to the microstrip line symmetry, the exciting field $\delta\mathbf{h}_{rf}$ possesses two components for each pump-

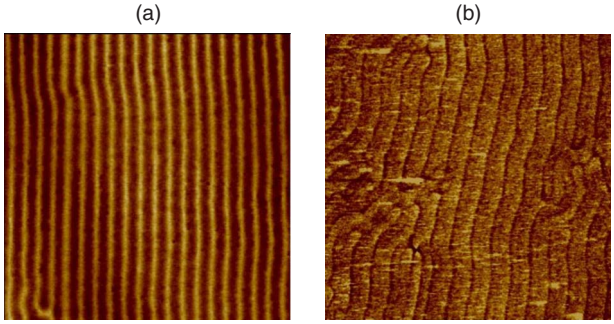

FIG. 7. (Color online) Zero-field MFM images of the domain pattern: (a) YIGBiLuAl monolayer, (b) Py/YIGBiLuAl bilayer. The image sizes are 30 μm$\times$30 μm.

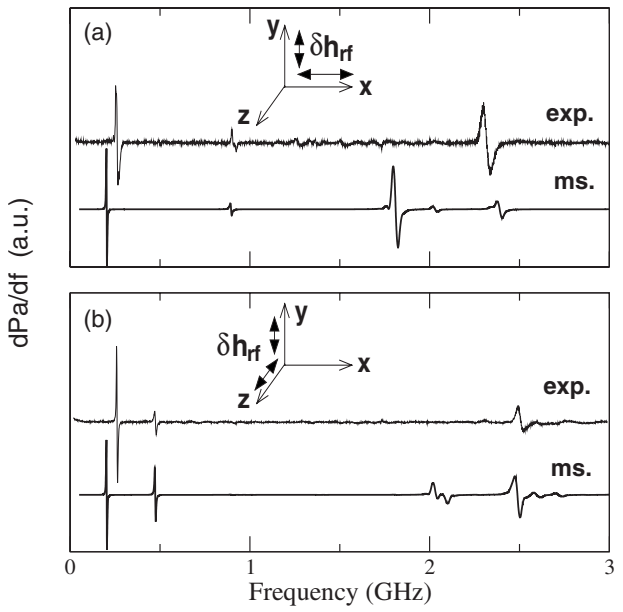

FIG. 8. Comparison between micromagnetic simulations (ms.) and experimental (exp.) zero-field derivative absorption power spectra for a YIGBiLuAl monolayer (t_1=0.5 μm): (a) stripe domains parallel to the microstrip line (z axis), and (b) stripe domains (z axis) perpendicular to the microstrip line (x axis).

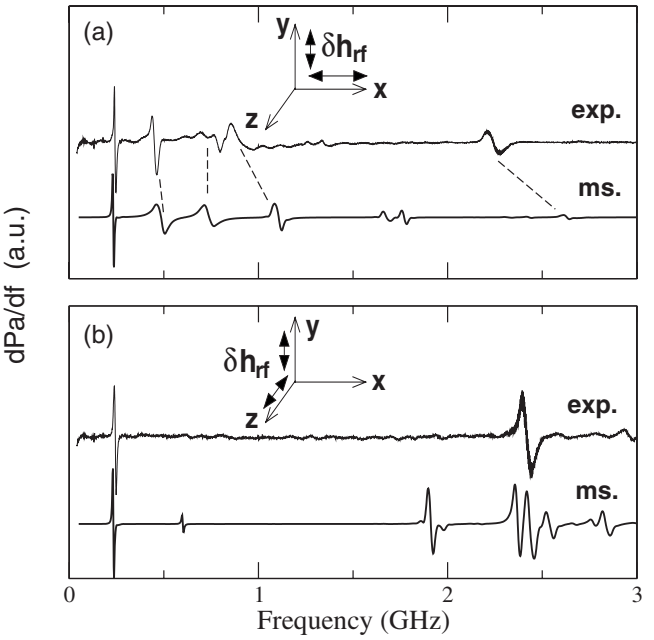

FIG. 9. Comparison between micromagnetic simulations (ms.) and experimental (exp.) zero-field derivative absorption power spectra for a Py/YIGBiLuAl bilayer (t_1=0.5 μm, t_2=30 nm): (a) stripe domains parallel to the microstrip line (z axis), and (b) stripe domains (z axis) perpendicular to the microstrip line (x axis).

ing configuration: a large in-plane one perpendicular to the microstrip line (x or z axis) and a weaker one perpendicular to the film (y axis), the stripe domains being oriented along the z axis. The computed spectra take into account a relative weightening between these two components in order to fit the experimental absorption curves.

The spectra consist in DW excitations below 1 GHz and domain excitations above 1.5 GHz. Several remarks can be made. (i) The computed spectra reproduced satisfactorily the two DW resonances (two lowest-frequency lying lines) and the volume domain resonance (highest-frequency lying line) for each pumping configuration. (ii) A surface domain mode exists in the computed spectra for each pumping configuration. For the parallel configuration [Fig. 8(a)], the surface domain mode results in an intensive line at f_r=1.81 GHz. For the perpendicular configuration [Fig. 8(b)], the surface domain mode corresponds to a weak signal at f_r=2 GHz. These surface domain modes are not revealed in the experimental spectra. One explanation can be advanced. The micromagnetic simulations are based on the perfect symmetry between the top and bottom surfaces of the monolayer. In the real single-crystal garnet film grown by LPE, several physical effects can induce a symmetry breaking between the two surfaces. Among them, the existence of a diffusion zone between the GGG substrate and the garnet film which possesses different magnetic properties has been reported.[23,24] Several computations (not presented here) performed by taking into account the presence of such a transient layer with different magnetic parameters (step variations in the magnetization induction or the uniaxial perpendicular anisotropy field) at the interface between the GGG substrate and the garnet film show a significative reduction in the line intensity associated with the surface domain mode accompanied by apparition of new weak resonance lines.

The experimental and computed derivative rf power absorption dP_a/df versus frequency within the frequency range [0.1–3 GHz] for the Py/YIGBiLuAl bilayer are presented in Fig. 9. For the parallel configuration [Fig. 9(a)], the experimental spectrum exhibits four resonance lines below 1 GHz, the third one being splitted, and an isolated resonance line at f_r=2.24 GHz. The spectrum computed by micromagnetic simulations reproduces these five resonance lines. The first four correspond to coupled modes between the DW inside the garnet film and the Py overcoat and the highest-frequency line is associated with a volume domain mode (similar to modes 1, 2, 3, 4, and 9 in Fig. 4). The spectral positions of the three first resonance lines appear very close between the experimental and the computed spectra. The resonance frequency of the fourth line is shifted toward the high frequency by about 20% in the computed spectrum. In a similar way, the resonance frequency of the volume domain mode is overestimated by the micromagnetic simulations. It should be noted that the computed spectrum reveals two signals at f_r=1.67 GHz and f_r=1.77 GHz, assigned to a surface domain mode localized at the lower surface and a high-order flexural DW mode which could correspond to a weak double line experimentally observed at f_r=1.27 GHz and f_r=1.35 GHz, respectively.

For the perpendicular configuration [Fig. 9(b)], the rf power spectrum is weakly modified with respect to the one of the garnet monolayer. The main difference is the disappearance of the Néel-type DW excitation. The micromagnetic simulations indicate a significative attenuation of this line in the bilayer system. It should be noted that the computed spectrum appears richer than the experimental one with the existence of multiple volume domain modes whose

spectral position lies between 2.37 and 2.54 GHz and a surface domain mode at $f_r = 1.91$ GHz.

As a conclusion, the micromagnetic simulations based on the assumption of an idealistic strong exchange coupling between the garnet film and the Py overcoat allow to explain a large number of magnetic excitations experimentally observed, in particular the coupled modes including DW oscillations and the gyromagnetic response of the Py film revealed in the parallel configuration. This finding extends the conclusion reported in Ref. 5 regarding the static properties of Fe/YIG-like bilayers which states that a strong direct interlayer exchange coupling is essential for explaining the domain pattern images.

IV. SUMMARY AND CONCLUSIONS

The static and high-frequency properties of in-plane/out-of-plane anisotropy bilayer systems have been investigated both numerically and experimentally. From the theoretical point of view, the 2D static micromagnetic simulations show that the in-plane magnetized overcoat allows to close the magnetic flux of the bilayer and induce deep modifications of the static magnetization configuration inside the out-of-plane anisotropy film (asymmetry between the top and bottom Néel caps, shift of Bloch DW core). The 2D dynamic micromagnetic simulations reveal the existence of multiple resonance lines ascribed to coupled modes inside the bilayer with a symmetry breaking with respect to its midplane. Intensive DW resonances within the out-of-plane anisotropy film coupled with the uniform gyromagnetic mode of the in-plane anisotropy film are thus pointed out. The features of the dynamic susceptibility spectra (number of lines, resonance frequencies, resonance line intensities, spatial distribution of modes) depend strongly on the individual film thicknesses.

From the experimental point of view, a YIGBiLuAl monolayer and a Py/YIGBiLuAl bilayer have been elaborated. The MFM images show that stripe domains exist in both systems, the zero-field stripe period being increased by adjunction of the Py overcoat. This behavior is accurately predicted by the static micromagnetic simulations based on a strong direct interlayer exchange coupling. The experimental zero-field power absorption spectra evidence clearly multiple coupled resonance modes, most of them being reproduced by the dynamic micromagnetic simulations.

It can be underlined that even for this simple bilayer system, the computation of dynamic susceptibility requires knowledge of twelve independent parameters. In this context, it is of crucial interest to determine them accurately by experimental means as it was made in this work. Nevertheless, some observed frequency shifts between the experimental and theoretical resonance frequencies could be partly attributed to accumulation of uncertainties regarding these parameters.

From these results, it can be concluded that the strong direct exchange coupling at the interface between the garnet film and the Py film appears predominant for such a bilayer system. An improved coupling model would demand a deeper analysis of the structural properties of the Py/garnet interface. Lastly, it should be mentioned that this powerful approach for computing the dynamic susceptibility spectra of nonuniform magnetized multilayer systems can be generalized to include other interfacial magnetic couplings [interlayer exchange coupling with bilinear (any value of J) and biquadratic terms, exchange interaction between ferromagnetic and antiferromagnetic layers].

*nicolas.vukadinovic@dassault-aviation.com

[1] S. D. Bader, Rev. Mod. Phys. **78**, 1 (2006).
[2] G. Ausanio, V. Ianotti, I. Lanotte, M. Carbucicchio, and M. Rateo, J. Magn. Magn. Mater. **226-230**, 1740 (2001).
[3] R. Brucas, H. Hafermann, M. I. Katsnelson, I. L. Soroka, O. Eriksson, and B. Hjorvarsson, Phys. Rev. B **69**, 064411 (2004).
[4] G. Beutier, G. van der Laan, K. Chesnel, A. Marty, M. Belakhovsky, S. P. Collins, E. Dudzik, J. C. Toussaint, and B. Gilles, Phys. Rev. B **71**, 184436 (2005).
[5] Y. S. Chun and K. M. Krishnan, J. Appl. Phys. **95**, 6858 (2004).
[6] M. Labrune and M. Carbucicchio, J. Magn. Magn. Mater. **269**, 203 (2004).
[7] A. Bollero, L. D. Buda-Prejbeanu, V. Baltz, J. Sort, B. Rodmacq, and B. Dieny, Phys. Rev. B **73**, 144407 (2006).
[8] N. Vukadinovic, M. Labrune, and J. Ben Youssef, Eur. Phys. J. B **50**, 593 (2006).
[9] N. Vukadinovic, O. Vacus, M. Labrune, O. Acher, and D. Pain, Phys. Rev. Lett. **85**, 2817 (2000).
[10] F. Hoffmann, A. Stankoff, and H. Pascard, J. Appl. Phys. **41**, 1022 (1970).
[11] B. Hillebrands, Phys. Rev. B **41**, 530 (1990).
[12] G. T. Rado and J. R. Weertman, J. Phys. Chem. Solids **11**, 315 (1959).
[13] L. Giovannini, S. Tacchi, G. Gubbiotti, G. Carlotti, F. Casoli, and F. Albertini, J. Phys.: Condens. Matter **17**, 6483 (2005).
[14] J. F. Cochran, B. Heinrich, and A. S. Arrott, Phys. Rev. B **34**, 7788 (1986).
[15] M. Takahashi, H. Nishida, T. Kobayashi, and Y. Sugita, J. Phys. Soc. Jpn. **34**, 1416 (1973).
[16] R. Suzuki, M. Takahashi, T. Kobayashi, and Y. Sugita, Appl. Phys. Lett. **26**, 342 (1975).
[17] M. Labrune and J. Miltat, J. Appl. Phys. **75**, 2156 (1994).
[18] N. Vukadinovic, J. Ben Youssef, and M. Labrune, Phys. Rev. B **66**, 132418 (2002).
[19] C. Kooy and U. Enz, Philips Res. Rep. **15**, 7 (1960).
[20] V. J. Fratello, S. E. G. Slusky, C. D. Brandle, and M. P. Novelli, J. Appl. Phys. **60**, 2488 (1986).
[21] D. Pain, M. Ledieu, O. Acher, A. L. Adenot, and F. Duverger, J. Appl. Phys. **85**, 5151 (1999).
[22] J. Ben Youssef, N. Vukadinovic, D. Billet, and M. Labrune, Phys. Rev. B **69**, 174402 (2004).
[23] C. Vittoria and H. Lessoff, Phys. Rev. Lett. **37**, 53 (1976).
[24] H. Dötsch, P. Röschmann, and W. Schiltz, Appl. Phys. **15**, 167 (1978).